Project 2241 | August 2023

SJSU SAN JOSÉ STATE UNIVERSITY

MTI MINETA TRANSPORTATION INSTITUTE

Fiber-Based Seismic Damage and Collapse Assessment of Reinforced Concrete Single-Column Pier-Supported Bridges Using Damage Indices

Yu-Fu Ko, PhD, PE
Jessica Gonzalez, EIT

CSUTC California State University Transportation Consortium

CALIFORNIA STATE UNIVERSITY LONG BEACH

Mineta Transportation Institute

Founded in 1991, the Mineta Transportation Institute (MTI), an organized research and training unit in partnership with the Lucas College and Graduate School of Business at San José State University (SJSU), increases mobility for all by improving the safety, efficiency, accessibility, and convenience of our nation's transportation system. Through research, education, workforce development, and technology transfer, we help create a connected world. MTI leads the Mineta Consortium for Transportation Mobility (MCTM) funded by the U.S. Department of Transportation and the California State University Transportation Consortium (CSUTC) funded by the State of California through Senate Bill 1. MTI focuses on three primary responsibilities:

Research

MTI conducts multi-disciplinary research focused on surface transportation that contributes to effective decision making. Research areas include: active transportation; planning and policy; security and counterterrorism; sustainable transportation and land use; transit and passenger rail; transportation engineering; transportation finance; transportation technology; and workforce and labor. MTI research publications undergo expert peer review to ensure the quality of the research.

Education and Workforce

To ensure the efficient movement of people and products, we must prepare a new cohort of transportation professionals who are ready to lead a more diverse, inclusive, and equitable transportation industry. To help achieve this, MTI sponsors a suite of workforce development and education opportunities. The Institute supports educational programs offered by the Lucas Graduate School of Business: a Master of Science in Transportation Management, plus graduate certificates that include High-Speed and Intercity Rail Management and Transportation Security Management. These flexible programs offer live online classes so that working transportation professionals can pursue an advanced degree regardless of their location.

Information and Technology Transfer

MTI utilizes a diverse array of dissemination methods and media to ensure research results reach those responsible for managing change. These methods include publication, seminars, workshops, websites, social media, webinars, and other technology transfer mechanisms. Additionally, MTI promotes the availability of completed research to professional organizations and works to integrate the research findings into the graduate education program. MTI's extensive collection of transportation-related publications is integrated into San José State University's world-class Martin Luther King, Jr. Library.

Report 23-19

Fiber-Based Seismic Damage and Collapse Assessment of Reinforced Concrete Single-Column Pier-Supported Bridges Using Damage Indices

Yu-Fu Ko, PhD, PE

Jessica Gonzalez, EIT

August 2023

A publication of the
Mineta Transportation Institute
Created by Congress in 1991

College of Business
San José State University
San José, CA 95192–0219

TECHNICAL REPORT DOCUMENTATION PAGE

1. Report No. 23-19	**2. Government Accession No.**	**3. Recipient's Catalog No.**
4. Title and Subtitle Fiber-Based Seismic Damage and Collapse Assessment of Reinforced Concrete Single-Column Pier-Supported Bridges Using Damage Indices		**5. Report Date** August 2023 **6. Performing Organization Code**
7. Authors Yu-Fu Ko, PhD, PE Jessica Gonzalez, EIT, Research Graduate Assistant		**8. Performing Organization Report** CA-MTI-2241
9. Performing Organization Name and Address Mineta Transportation Institute College of Business San José State University San José, CA 95192–0219		**10. Work Unit No.** **11. Contract or Grant No.** ZSB12017-SJAUX
12. Sponsoring Agency Name and Address State of California SB1 2017/2018 Trustees of the California State University Sponsored Programs Administration 401 Golden Shore, 5th Floor Long Beach, CA 90802		**13. Type of Report and Period Covered** **14. Sponsoring Agency Code**
15. Supplemental Notes		

16. Abstract

Near-fault earthquakes can have major effects on transportation systems due to the structural damage they impose on bridges. Therefore, it is imperative to assess the seismic damage of bridges appropriately, and this research focuses on reinforced concrete (RC) bridges. This research advances the seismic performance assessment of RC single-column pier-supported bridges with flexural failure under near-fault ground motion by use of ductility coefficients and damage indices. The methodology included modeling fiber-based nonlinear beam-column elements to simulate the damage development process of RC bridge piers under earthquake loadings, considering the global buckling of longitudinal steel bars, examining the cracking and spalling of cover concrete, and analyzing the effects of bond-slip. The tensile strain represented the damage of the longitudinal bars while the compression strain represented the cover concrete damage. Two innovative nonlinear fiber-based finite element models (FEMs) were developed: Model 1 (bond-slip excluded) and Model 2 (bond-slip included). Nonlinear static cyclic pushover analyses and nonlinear response history analyses were conducted. The simulation results were compared with available pseudo-dynamic test results. Model 1 provided a more ideal prognosis on the seismic performance of RC single-column pier-supported bridges under near-fault ground motion. The proposed damage indices can indicate the damage state at any stage and the gradual accumulation of damage in RC bridge piers, which are more convincing than most other indices in the literature. The proposed fiber-based nonlinear FEMs, together with the use of ductility coefficients and proposed damage indices, can also assist engineers and researchers in simulating the seismic behavior and assessing the damage state of RC bridge columns in a computationally effective manner which can empower engineers to identify and prioritize RC bridges for seismic retrofit and maintenance.

17. Key Words Reinforced concrete bridges, Finite element method, Earthquake engineering, Dynamic structural analysis, Seismicity	**18. Distribution Statement** No restrictions. This document is available to the public through The National Technical Information Service, Springfield, VA 22161.		
19. Security Classif. (of this report) Unclassified	**20. Security Classif. (of this page)** Unclassified	**21. No. of Pages** 46	**22. Price**

Form DOT F 1700.7 (8–72)

DOI: 10.31979/mti.2023.2241

Mineta Transportation Institute
College of Business
San José State University
San José, CA 95192–0219

Tel: (408) 924–7560
Fax: (408) 924–7565
Email: mineta-institute@sjsu.edu

transweb.sjsu.edu/research.2241

Acknowledgments

This research work was financially supported by the Mineta Transportation Institute (MTI) for Transport Year 5, 2022. The research team would like to thank MTI for the support received to accomplish this research.

Contents

List of Figures

List of Tables

Executive Summary

California has been host to a whole series of moderate and larger earthquakes, which affect the lives of millions of people. Reinforced concrete (RC) bridges are vital components of transportation systems and vulnerable during major earthquakes. To ensure safety and performance of RC bridges, it is imperative to propose research on bridge seismic retrofit and maintenance in California. This research project will be successful in meeting this specific need in California that will benefit and contribute to Californians, diverse leaders, practitioners, and society to provide sustainable transportation bridge infrastructures to protect public safety. This research project evaluated and analyzed the seismic performance of RC bridges. RC bridge column piers that underwent higher level damages will be identified and prioritized for seismic retrofit and bridge maintenance.

The purpose of this research is to numerically assess the seismic performance of reinforced concrete (RC) single-column pier-supported bridges with combined damage mechanisms including concrete cracking and spalling, longitudinal reinforcing bar buckling, and bond-slip between longitudinal reinforcing bars and concrete. Two different advanced finite element models (FEMs)—Model 1 (excluding bond-slip) and Model 2 (including bond-slip)—were proposed to observe the effects of bond-slip material and to compare their ductile responses with ductility coefficients and damage indices.

The analysis of the fiber-based FEMs was conducted using the Open System for Earthquake Engineering Simulation (OpenSees) program. The rectangular cross section of the RC bridge column consisted of confined core concrete fibers, unconfined cover concrete fibers, and longitudinal reinforcing steel fibers. The unconfined concrete fibers were discretized and monitored in 36 locations, and the steel fibers were analyzed in 16 locations. The confined and unconfined concrete regions of the bridge column were accounted for when developing the FEMs to consider the effect of closed steel hoops (transverse reinforcing bars) on the concrete.

Two FEMs were developed: Model 1 (excluding bond-slip) and Model 2 (including bond-slip) to study the effect of bond-slip. Both models have uniaxial nonlinear fibers represented in OpenSees as UniaxialMaterial to represent the stress-strain hysteresis behaviors of concrete and reinforcing steel. Section aggregated with elastic shear for concrete was not considered as it is assumed that shear failure does not govern the bridge column with flexural failure in this research. The bridge column of both models was formed by finite element nodes, and additional nodes were placed between nodes 1 and 2 to refine the element length. Furthermore, for Model 2, a zero-length section element was created at the base of the RC bridge column between nodes 1 and 100 to observe the bond-slip effect. Yielding and damage were anticipated under strong seismic loadings. Therefore, nonlinear fiber-based and displacement-based beam-column elements were used between nodes to represent the bridge columns for both models. Nonlinear fiber-based and displacement-based beam-column elements with distributed plasticity were used in the proposed models as they allow for the growth of nonlinearities anywhere along the member, precisely capturing the seismic responses of RC bridge columns.

The damage index of RC bridges is numerically defined in ranges corresponding to the structural damage based on NCHRP Synthesis, which is adopted in this research. The fiber-based damage models are coded in the OpenSees program to conduct nonlinear analyses of RC bridge columns and to measure ductility coefficients and material damage indices. The RC bridge column and cross sections are divided into fiber cells which are assigned uniaxial constitutive models that have nonlinear material properties representing stress-strain hysteresis models for concrete and longitudinal rebar. Three different regions are assigned within the RC sections: cover concrete, core concrete, and reinforcing steel. The reinforcing steel material used is based on the steel model to simulate the reinforcing bars in the bridge columns. The steel model takes into consideration the mechanical effects of strain softening, compression buckling, and tensile fracture of the reinforcement bars. Bar buckling has a significant influence on the constitutive model of reinforcing bars and can therefore affect the seismic response of RC structures. The OpenSees concrete02 material model is applied in this fiber-based model. An advantage of the proposed FEMs is that they provide continuous modeling of cover concrete spalling progress which allows us to identify when spalling and significant spalling starts.

Nonlinear static cyclic pushover analyses and nonlinear response history analyses were conducted. The simulation results were compared with available pseudo-dynamic testing results. The results demonstrated that under near-fault ground motion, Model 2 (including bond-slip) underestimated the lateral stiffness, longitudinal reinforcing steel bar strain, and cover concrete strain. When compared with the pseudo-dynamic testing results, Model 1 (excluding bond-slip) was found to be most optimal to assess the seismic performance of RC single-column pier-supported bridges with flexural failure under near-fault ground motion. The proposed assessment method will avoid overconservative condition ratings of RC bridge columns. The proposed numerical FEMs improve the accuracy of the predictions of nonlinear flexural failure behaviors of RC single-column pier-supported bridges during seismic events. The proposed damage indices can indicate the damage state at any stage and the gradual accumulation of damage in RC bridge piers, which are more comprehensive than other indices in the literature. The proposed damage index can reasonably reflect the damage states at the onset of spalling, significant spalling, bar buckling, and failure in accordance with the experimental results. The proposed fiber-based nonlinear FEMs together with the use of ductility coefficients and proposed damage indices can also assist engineers and researchers in simulating the seismic behavior and assessing the damage state of RC bridge piers in a computationally effective manner.

1. Introduction

Bridges play an important role in national development as they are a critical component of a nation's infrastructure. Earthquake-induced damage on bridges has major impacts on transportation networks. Hence, it is essential to assess the seismic damage of bridge components accurately. There is a dense network of faults in California and, as a result, increased seismic activity and risk. Therefore, there are concerted efforts and motivations to predict seismic behavior and quantify its resulting damage. Near-fault earthquakes can cause a permanent displacement offset along the fault and produce pulse-like velocity waveforms that are potentially destructive to structures, which makes the study of near-fault ground-motion characteristics an important topic to the engineering community.

Various experimental test results and numerical simulations of RC bridge columns under near-fault earthquakes have been considered [1, 2–8] such as Chang who performed pseudo-dynamic testing of two bridge columns under cyclic loading to estimate their shear strength, flexural strength, and ductility [1]. Loh et al. evaluated the structural response attributes of near-fault ground motion by modeling a nonlinear hysteretic model [2]. An effective method used to quantify the level of structural damage caused by an earthquake is through damage indices. Damage indices are used to numerically measure the level of damage on structures caused by earthquake loadings which are in turn used in seismic retrofit and maintenance decisions. Many seismic damage indices have been previously reviewed in the literature [9–14, 17]. Park and Ang proposed a damage index that combined deformation and energy dissipation, but their damage index equation includes the ultimate deformation coefficient which, they admit, there is no reliable method to determine in RC "especially when shear deformation and bond slippage may be dominant" [10,11]. Babazadeh et al. use 3D continuum-based finite element simulations to estimate intermediate damage limit states, but they do not take into account bond-slip effects because a perfect bond between the rebar and concrete was assumed in their model [15,16]. Su's research conducted a fiber-based nonlinear finite element analysis to simulate nonlinear responses of reinforced concrete (RC) bridge columns where tensile strain and low-cycle fatigue were used to assess damage in the reinforcing steel, and the compressive strain of concrete was used to assess the damage of concrete [17]. Su used the five performance levels shown in Table 1 to measure the damage visually [18], damage models [19–23], and the NCHRP Synthesis 440 [24] to classify bridge column damage and performance levels as shown in Table 2. This method is adopted in this research to investigate the seismic performance of RC single-column pier-supported bridges near ground motion through the use of damage indices.

However, damage indices proposed by prior literatures have not been developed to deal explicitly with bond-slip effect and various combined damage mechanisms observed through the experimental tests for RC bridge columns. This proposed research studies will fill the gaps. The purpose of this research is to numerically assess the seismic performance of reinforced concrete (RC) single-column pier-supported bridges with combined damage mechanisms including bond-slip between the concrete and the longitudinal reinforcing bars [25–28], buckling of the longitudinal reinforcing bars [29–31], and concrete cracking and spalling [31–32]. Two different advanced finite element models (FEMs), Model 1 (excluding bond-slip) and Model 2 (including bond-slip), were proposed to observe the effects of bond-slip material and to compare their ductile responses with ductility coefficients and damage indices. The simulation results were compared with available pseudo-dynamic testing results [1]. The RC bridge column analyzed in this research is fixed at the base and free at the top, as shown in Figure 1, which assessed the seismic performance and damage of RC bridge RC columns based on various ductility coefficients and the proposed damage indices.

Figure 1. Typical Inelastic Regions and Bond-Slip Locations in Ductile RC Single-Column Pier-Supported Bridges

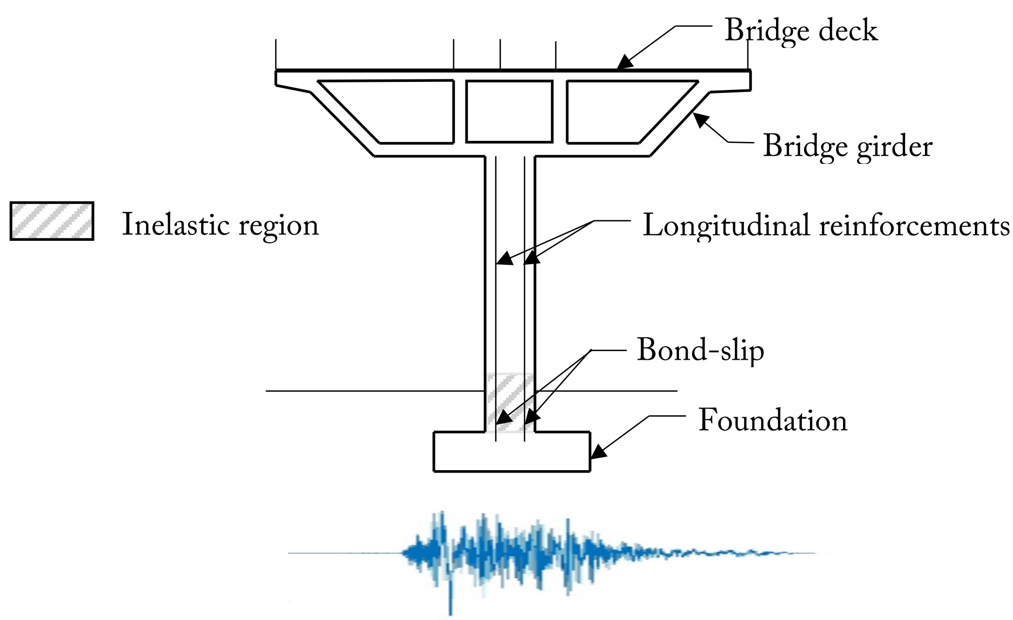

2. Pseudo-dynamic Test: Specimen Description and Testing Procedure

The bridge column chosen for this research is found in Chang et al.'s [1] research, which performed pseudo-dynamic tests on two as-built columns (Specimen A and B) at a 2/5 decreased scale that was designed according to the 1995 version of the Taiwan Bridge Design Code, based on 1992 AASHTO Specifications. The bridge columns have a height of 3.25 m and cross section 0.75 m by 0.60 m with a 25 mm concrete cover. The bridge column has an axial compressive load of 680 kN. A total of 32 No. 6 longitudinal bars were evenly distributed throughout the height of the bridge column with design yield strength f_y = 420 MPa (actual yield strength from testing was 500 MPa). Concrete compressive strength was f'_c = 21 MPa at 28 days (actual f_y = 23 MPa). The transverse reinforcing bars were No. 3 stirrups with a design yield strength of f_y = 280 MPa (actual f_y = 350 MPa) spaced at 100 mm. The transverse reinforcement also included five confining crossties. The hoops and crossties were anchored at their two ends at 90° and 135°, respectively. The longitudinal bars' ratio was 1.95% and the transverse reinforcing bars' ratio was 1.04%.

The specimens underwent horizontal ground acceleration from the Chi-Chi earthquake in Taiwan. The ground motion was obtained from station TCU075, and the PGA was scaled up to 0.8 g. Specimen A was subjected to reverse cyclic loading to obtain the maximum force, maximum lateral displacement, and maximum ductility capacity of both specimens. Specimen B was subjected to pseudo-dynamic loading to obtain accurate seismic responses and seismic demands of RC bridge columns under near-fault ground motions. The displacement control mode was used for the experimental tests directed, and the pseudo-dynamic results of Specimen B were then correlated and graded with the simulation results of the proposed nonlinear fiber-based finite element damage models.

3. Nonlinear Fiber-Based Finite Element Models

The analysis of the fiber-based FEMs was conducted using the Open System for Earthquake Engineering Simulation (OpenSees) program [21]. The rectangular cross section of the RC bridge column consisted of confined core concrete fibers, unconfined cover concrete fibers, and longitudinal reinforcing steel fibers, as shown in Figure 3a. The unconfined concrete fibers were discretized and monitored in 36 locations, and the steel fibers were analyzed in 16 locations whose coordinates are shown in Figure 2. The confined and unconfined concrete regions of the bridge column were accounted for when developing the FEMs to consider the effect of closed steel hoops (transverse reinforcing bars) on the concrete.

Two FEMs were developed: Model 1 (excluding bond-slip) and Model 2 (including bond-slip) to study the effect of bond-slip. Both models have uniaxial nonlinear fibers represented in OpenSees as UniaxialMaterial to represent the stress-strain hysteresis behaviors of concrete and reinforcing steel. Section aggregated with elastic shear for concrete was not considered as it is assumed that shear failure does not govern the bridge column with flexural failure. The bridge column of both Models was formed by finite element nodes, and additional nodes were placed between nodes 1 and 2 to refine the element length. Furthermore, for Model 2, a zero-length section element was created at the base of the RC bridge column between nodes 1 and 100 to observe the bond-slip effect. Yielding and damage of the bridge column were anticipated under strong seismic loadings. Therefore, nonlinear fiber-based and displacement-based beam-column elements were used between nodes to represent the bridge columns for both models. Nonlinear fiber-based and displacement-based beam-column elements with distributed plasticity were used in the proposed models as they allow for the growth of nonlinearities anywhere along the member, precisely capturing the seismic responses of RC bridge columns.

Figure 2. Fiber Numbering Layout in the Cross Section

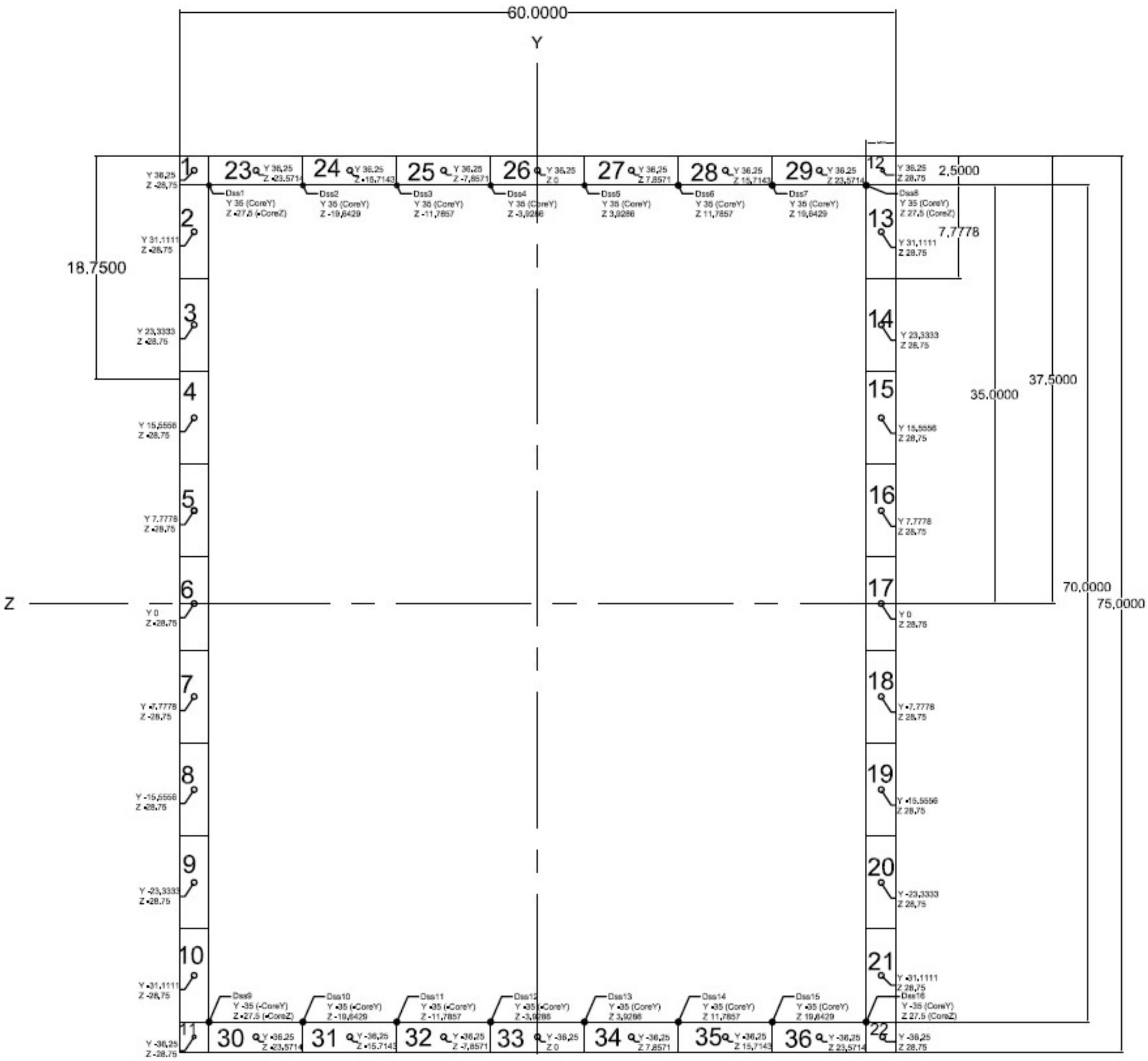

3.1 Model 1 (Excluding Bond-slip)

The finite element models of the RC bridge column were assembled with the use of nonlinear fiber-based and displacement-based beam-column elements. The uniaxial concrete material Concrete02 with tensile strength and linear tension softening was the material object utilized for the confined and unconfined concrete of the bridge column modeling. The uniaxial material ReinforcingSteel [33] was employed in the RC fiber section to model the longitudinal reinforcing steel bars. We employed the following parameters.

Unconfined concrete: the concrete compressive strength at 28 days (f'_c = -23.0 MPa), the concrete strain at maximum strength (ε_0 = -0.002), the initial slope for the compressive stress-strain curve ($E_c = 4700\sqrt{f'_c}$ = 22,540.0 MPa), the concrete crushing strength (f_{cu} = 0:0 MPa), the concrete strain at crushing strength (ε_{cu} = -0.004), the ratio between unloading slope at ε_{cu} and initial slope (λ = 0.1), the tensile strength of the concrete ($f_t = 0.59\sqrt{f'_c}$ = 2.83 MPa), the tensile strain of 0.00012 at f_t, and the tension softening stiffness ($E_{ts} = E_c/10$ = 2254.0 MPa).

Confined concrete: the concrete compressive strength at 28 days (f'_{cc} = -24.8 MPa), the concrete strain at maximum strength (ε_{cc} = 0.0061), the initial slope for compressive stress–strain curve ($E_c = 5000\sqrt{f'_{cc}}$ = 24,900.0 MPa), the concrete crushing strength ($f_{cu} = 0.4f'_{cc}$ = 9.9 MPa), the concrete strain at crushing strength (ε_{cu} = -0.014), the ratio between unloading slope at ε_{cu} and initial slope (λ = 0.1), the tensile strength of the concrete ($f_t = 0.59\sqrt{f'_{cc}}$ = 2.94 MPa), and the tension softening stiffness (slope of the linear tension softening branch) ($E_{ts} = E_c/10$ = 2490.0 MPa).

Longitudinal rebars: the yield strength in tension (f_y = 420 MPa), the ultimate strength ($f_u = 1.19f_y$), the initial elastic tangent modulus (E_s = 200,000.0 MPa), tangent at initial strain-hardening modulus (E_{sh} = 7000.0 MPa), strain corresponding to initial strain hardening (ε_{sh} = 0.008), and strain at peak stress (ε_{su} = 0.14).

The buckling of longitudinal rebar was considered (as in Gomes and Appleton [29]; Dhakal and Maekawa [30]). ReinforcingSteel material with a slenderness ratio of $l_{SR} = 1.5 * L_u/d_b = 1.5 * s/d_b$ was adopted, where L_u, d_b, and s are the unsupported length, diameter of the circular cross section of the longitudinal reinforcing bars, and the spacing of transverse reinforcing bars, respectively. The buckled stress σ_b was computed as follows:

$$\sigma_b = \gamma f_u - \frac{\Omega_b + \gamma}{1+\gamma}(\gamma f_u - \sigma);\ \Omega_b = \beta\frac{\sqrt{32}}{(3\pi\, l_{SR}\sqrt{\varepsilon_s - \varepsilon_y})} \quad (1)$$

with an amplification factor β = 1.0, a buckling reduction factor r = 0.0, and a buckling constant γ = 0.5 implemented. Additionally, σ_b, ε_y, and f_u represented the buckled stress, yield strain, and ultimate strength of the ReinforcingSteel material in tension, respectively. The plastic hinge length (Lp) per Caltrans Seismic Design Criteria is defined as follows:

$$L_p = 0.08L + 0.022\, f_{ye}\, d_{bl} \geq 0.044\, f_{ye}\, d_{bl}\ (\text{mm, } f_{ye} \text{ in MPa}) \quad (2)$$

where L is the member length from the point of maximum moment to the point of contra-flexure, f_{ye} is the expected yield strength for longitudinal reinforcement, and d_{bl} is the longitudinal bar reinforcement's nominal diameter. The analytical plastic hinge length is the equivalent length of column where the plastic curvature is assumed constant when estimating the plastic rotation. However, nonlinear fiber-based and displacement-based beam-column elements in OpenSees were employed in the current study to consider the spread of plasticity along the element instead of using a lumped plastic hinge with the analytical plastic hinge length. Additionally, as shown in Figures 6 and 8, six displacement-based beam-column elements were favored after performing the element refinement studies and convergence tests. Furthermore, the Gauss-Lobatto quadrature rule was used for default integration along the element.

3.2 Model 2 (Including Bond-slip)

Model 2 is differentiated with an added zero-length section to represent bond-slip, as shown in Figure 6b. The zero-length section element was assigned between node 1 and node 100. The translational degree-of-freedom of node 100 was constrained to node 1. The concrete material within the zero-length section is the same as the fiber-based beam-column elements, but the reinforcing steel in the zero-length section uses Bond_SP01 uniaxial material to capture the bond-slip effects at the column-to-footing intersection [28].

The monotonic bar stress (σ) vs. loaded-end slip (S) response curve in Bond_SP01 is shown in Figure 3b and defined in the following Equations (3)–(5):

$$\sigma = \begin{cases} KS, if\ S\ \leq S_y \\ \tilde{\sigma}\ x\ (\sigma_u\ - \sigma_y) +\ \sigma_y, if\ S > S_y \end{cases} \quad (3)$$

$$\tilde{\sigma} = \frac{\frac{\tilde{S}}{\mu - \tilde{S}}}{[(\frac{1}{\mu x b})^{Rc} + (\frac{\tilde{S}}{\mu - \tilde{S}})^{Rc}]^{1/Rc}} \quad (4)$$

where $\tilde{\sigma} = \sigma - \sigma_y / \sigma_u - \sigma_y$ is the normalized bar stress, $\tilde{S} = (S - S_y)/S_y$ is the normalized bar slip, $\mu = (S_u - S_y)/S_y$ is the ductility coefficient, and *b* is the stiffness reduction factor. The $\tilde{\sigma}$ is the ratio of the initial slope of the curvilinear portion at the onset of yielding to the slope in the elastic region, *K*. Furthermore, σ_y depicts the yield strength, and σ_u represents the ultimate strengths of the steel reinforcing bar. S_y is the loaded end-slip when σ_y is the bar stress, and S_u is the same when the bar stress is σ_u. S_y is computed as follows:

$$S_y = 0.4\left[\frac{d_b}{4}\frac{Fy}{\sqrt{f'_c}}\ (2\alpha + 1)\right]^{1/\alpha} + 0.34\ (mm, Mpa) \quad (5)$$

Additionally, to take the hysteretic responses of bar stress vs loaded-end slip into account, the coefficient R_c defines the shape of the reloading curve and usually ranges from 0.5–1.0. A smaller R_c value is associated with significant pinching behavior, while a value of 1.0 will render no pinching effect. For Bond_SP01, we used: the local bond-slip relation (α = 0.4), rebar slip at the loaded end at the bar fracture strength ($S_u = 30S_y$), the stiffness reduction factor (b = 0.05), and coefficient to reflect the pinching effect (R_c = 0.23).

Figure 3. (a) Fiber Element Discretization of the Cross Section of the RC Bridge Column; (b) Envelope Curve of the Bars Stress Vs. Loaded-End Slip Relationship as Modeled in Bond_Sp01 [28]

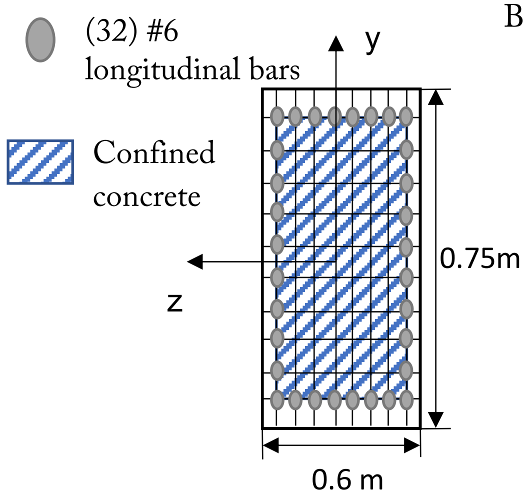

(a)

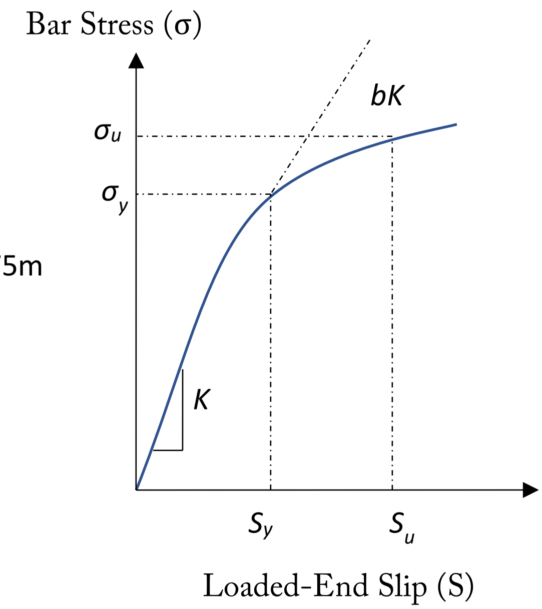

(b)

4. Damage Models of Material

Damage of RC bridges can be assessed and measured visually as shown in Table 1 per Stone and Taylor [19]. Stone and Taylor presented five levels of qualitative and quantitative performance descriptions to measure the state of the RC bridge. Furthermore, the damage index of RC bridges is numerically defined in ranges corresponding to the structure damage as seen in Table 1 [19], which is based on the NCHRP Synthesis [24] and is used in this research. Some of the qualitative guidelines include crack widths and their length. The concrete crack widths are associated with the tensile strain of longitudinal bars, for which Goodnight et al. [20] calculated the corresponding steel strain values for various crack widths. The first significant sign of damage in RC bridge columns is the onset of the yielding of longitudinal steel bars in tension, which is shown in Table 2 [24] as Level II. Table 1 shows that the onset of concrete spalling corresponds to the crack length extending to one-tenth of the section depth in Level III, and significant spalling corresponds to concrete crack widths larger than 2 mm that extend over half of the cross section in Level IV.

Figure 4. Section Damage Indices [17]

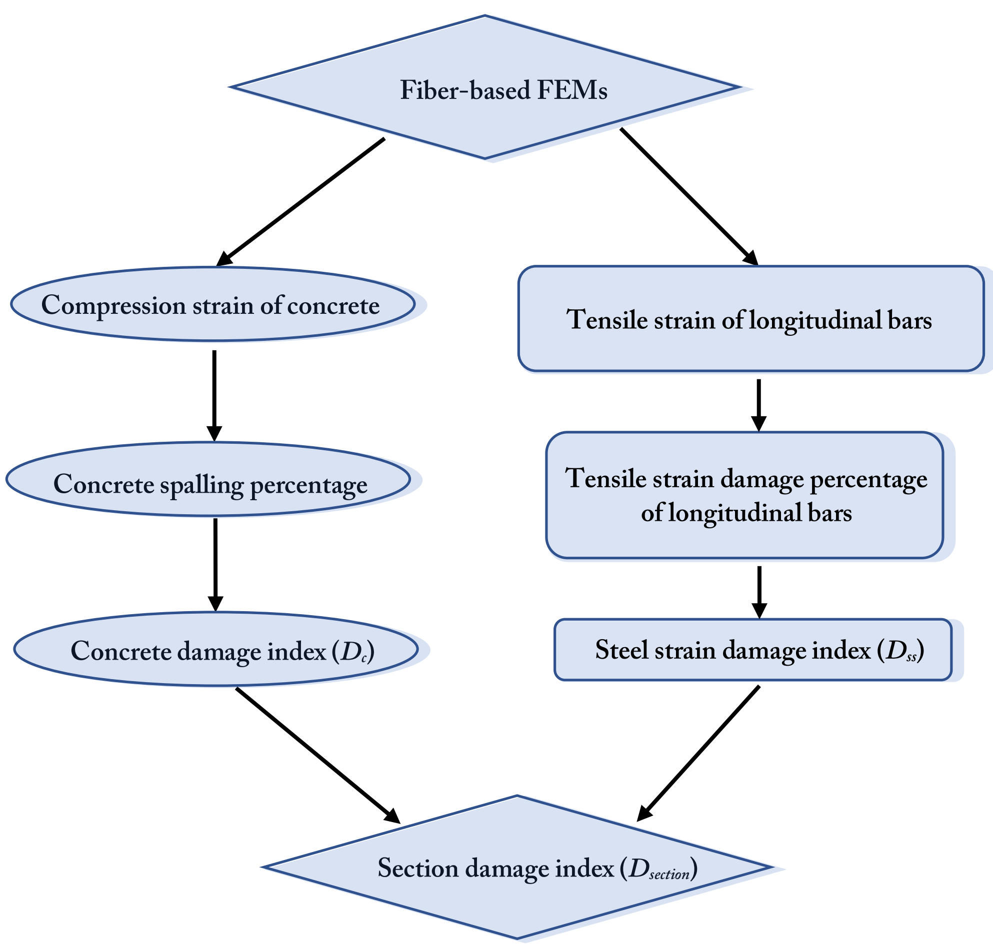

4.1 Fiber-Based Damage Model

The proposed fiber-based damage models in this research were coded in the Open System for Earthquake Engineering Simulation (OpenSees) program [21] to conduct nonlinear analyses and to measure the damage state of RC bridge columns. The RC bridge column and its cross sections were divided into fiber cells which are assigned uniaxial constitutive models that have nonlinear material properties representing stress-strain hysteresis models for concrete and longitudinal rebar. RC cross sections are assigned as: cover concrete, core concrete, and reinforcing steel.

ReinforcingSteel [33] steel material was used to simulate the longitudinal reinforcing bars in the bridge columns. The steel model takes into consideration the mechanical effects of strain softening, compression buckling, and tensile fracture of the reinforcement bars. Bar buckling has a significant influence on the constitutive model of reinforcing bars and can therefore affect the seismic response of RC structures [29].

The OpenSees concrete02 material model employed in these fiber-based FEMs was developed by Yassin [35]. The advantage of the proposed FEMs could provide continuous modeling of cover concrete spalling progress, which allows us to identify when onset spalling, significant spalling, and full spalling starts.

Table 1. Bridge Performance Assessment (Stone and Taylor [19])

Level	Performance level	Qualitative performance characterization	Quantitative performance characterization
I	Cracking	Onset of hairline cracks	Cracks hardly visible
II	Yielding	Theoretical first yielding of longitudinal reinforcement	Crack widths < 1 mm
III	Initiation of local mechanism	Initiation of inelastic deformation, onset of concrete spalling, development of diagonal cracks	Crack widths of 1–2 mm, length of spalled region > 1/10 of the cross-section's depth
IV	Full development of local mechanism	Wide and extended cracks, significant spalling over local mechanism region	Crack widths > 2 mm, diagonal cracks extend over 2/3 of the cross-section's depth, length of spalled region > 1/2 of the cross-section's depth
V	Strength degradation	Buckling of main reinforcement, rupture of transverse reinforcement, crushing of core concrete	Crack widths > 2 mm in core concrete

Table 2. Definitions of Damage Index Levels (NCHRP Synthesis [24])

Level	Damage Classification	Damage Value	Description	Performance Condition
I	None	$D < 0.1$	Onset of hairline cracks	Fully operational
II	Minor	$0.1 \leq D < 0.2$	Crack widening, first yielding of reinforcement	Operational
III	Moderate	$0.2 \leq D < 0.4$	Onset of cover concrete spalling	Limited damage
IV	Major	$0.4 \leq D < 0.6$	Significant spalling	Life safety
V	Local Failure/Collapse	$0.6 \leq D < 1.0$	Buckling of reinforcement, crushing of core concrete	Collapse

Figure 5. Cover Concrete Spalling Percentage Definition [17]

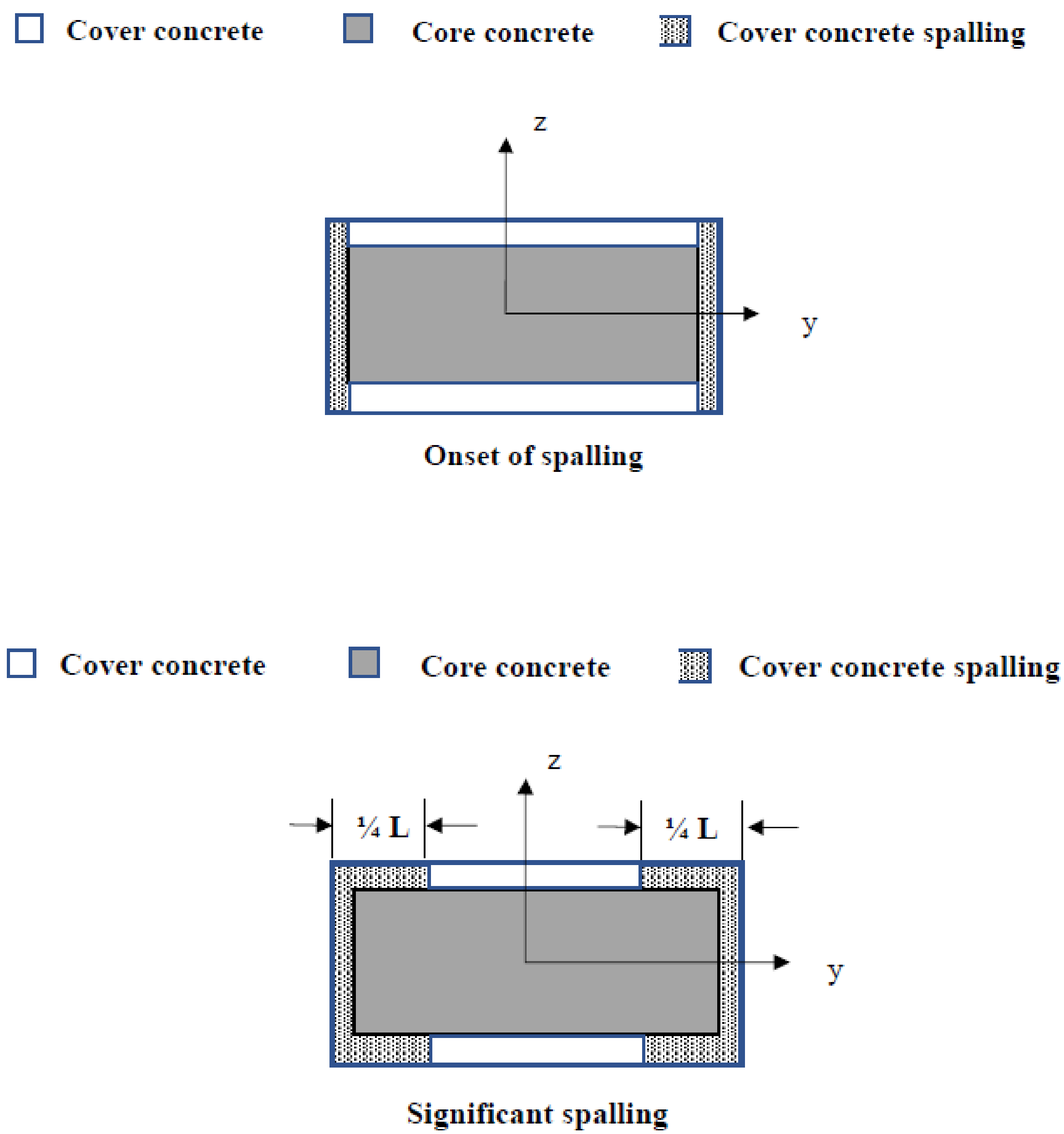

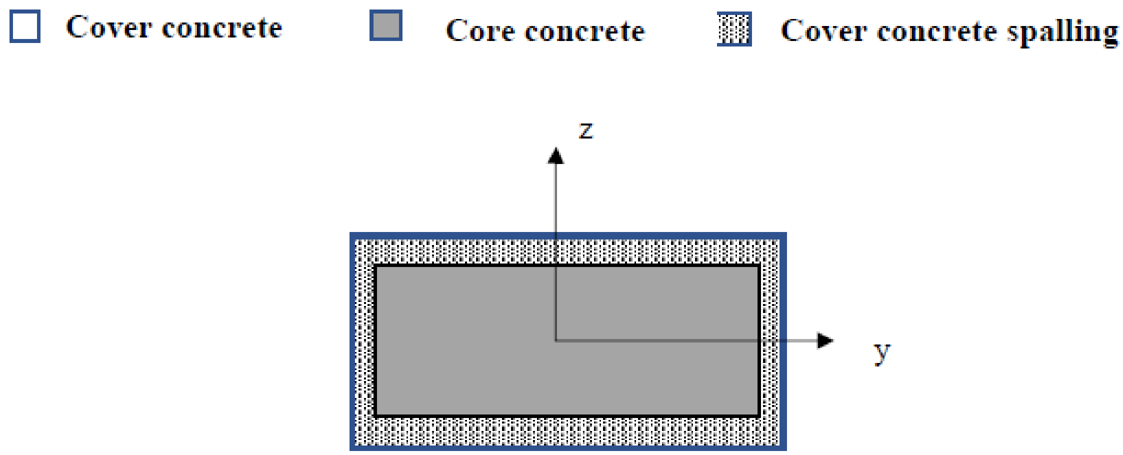

Full spalling

4.2 Concrete Damage

The extent of cover concrete spalling is reflective of the deterioration of RC cross sections and, thus, indicative of the damage sustained by RC bridge columns. The section damage of concrete is defined as follows:

$$D_c = \begin{cases} p/p_1 * D_{s1}, p < p_1 \\ D_{sc1} + (p - p_1)/(p_2 - p_1) * (D_{sc2} - D_{sc1}), p_1 < p \leq p_2 \\ D_{sc2} + (p - p_2)/(p_3 - p_2) * (D_{sc3} - D_{sc2}), p_2 < p \leq p_3 \end{cases} \quad (6)$$

where p is the percentage of cover concrete spalling which is illustrated in Figure 5 [17]. The damage indices D_{sc1} to D_{sc3} are equal to 0.2, 0.4, and 0.6, respectively. The compression strain of -0.005 was used to pinpoint the start of the spalling of cover concrete [15]. At each time step, the concrete damage was evaluated as onset spalling, significant spalling, or full spalling, as illustrated in Figure 5. For instance, the percent, p_1, during the onset of spalling, was the number of fibers that reached or surpassed the strain threshold of -0.005 over the total number of fibers. The p_1, p_2, and p_3 of the RC rectangular section were determined to be 50%, 72%, and 100% of the rectangular section, respectively.

4.3 Steel Strain Damage

The strain-based damage of reinforcing steel bars in RC bridge columns is defined as follows:

$$D_{ss} = \begin{cases} \frac{\varepsilon_b}{\varepsilon_y} * D_{s1}, \varepsilon_s < \varepsilon_y \\ D_{s1} + (\varepsilon_s - \varepsilon_y)/(\varepsilon_{c1} - \varepsilon_y) * (D_{s2} - D_{s1}), \varepsilon_y \le \varepsilon_s < \varepsilon_{c1} \\ D_{s2} + (\varepsilon_s - \varepsilon_{c1})/(\varepsilon_{c2} - \varepsilon_{c1}) * (D_{s3} - D_{s2}), \varepsilon_{c1} \le \varepsilon_s < \varepsilon_{c2} \\ D_{s3} + (\varepsilon_s - \varepsilon_{c2})/(\varepsilon_{bb} - \varepsilon_{c2}) * (D_{s4} - D_{s3}), \varepsilon_{c1} \le \varepsilon_s < \varepsilon_{bb} \\ D_{s4} + (\varepsilon_s - \varepsilon_{c3})/(\varepsilon_u - \varepsilon_{bb}) * (D_{s5} - D_{s4}), \varepsilon_{bb} \le \varepsilon_s < \varepsilon_u \\ D_{s5}, \varepsilon_s \ge \varepsilon_u \end{cases} \quad (7)$$

The ultimate strain of the longitudinal steel, ε_{u}, is set to 0.1 in this research. The ε_{c1} and ε_{c2} are the strain values of longitudinal bars of 0.01 and 0.02 corresponding to the crack widths of 1 mm and 2 mm per Goodnight et al. [20]. The damage classifications D_{s1} to D_{s5} are defined as 0.1, 0.2, 0.4, 0.6, and 1.0, respectively. In addition, the buckling strain is defined as:

$$\varepsilon_{bb} = 0.03 + 700 p_{sh} \frac{f_{yh}}{E_s} - 0.1 \frac{P}{f'_c A_g} \quad (8)$$

4.4 Section Damage Index

Once the concrete damage and steel damage values were determined, the maximum value is taken as the section damage index, as expressed in Equation 9 and Figure 4.

$$D_{section} = max\{Avg. D_{ss}, D_c\} \quad (9)$$

5. Nonlinear Static Cyclic Pushover Analysis

Model 1 (excluding bond-slip) and Model 2 (including bond-slip) both underwent nonlinear static cyclic pushover analysis with displacement control with a constant axial compressive load of P = 680 kN, as shown in Figure 6a and 6b. Nonlinear cyclic pushover analysis was performed to assess the strength and ductility capacities of the RC bridge column. The loading sequences implemented are shown in Table 3 per Chang et al [1]. Additionally, the *P*-Delta effect was accounted for. The displacement ductility capacity was defined as follows:

$$\mu_{\Delta,\text{capacity}} = \Delta_{max}/\Delta_y \quad (10)$$

The equation above consists of Δ_y, the yield displacement, and Δ_{max}, the maximum displacement. The results are shown in Table 4 and illustrated in Figure 7. In Figure 7, the lateral force vs. lateral displacement hysteresis curve of both models is shown. Figure 7b demonstrates that Model 2 has less saturated hysteretic loop and significant pinching effect due to bond-slip effect.

Figure 6. Nonlinear Static Cyclic Pushover Analysis of (a) Model 1 (Excluding Bond-Slip) and (b) Model 2 (Including Bond-Slip)

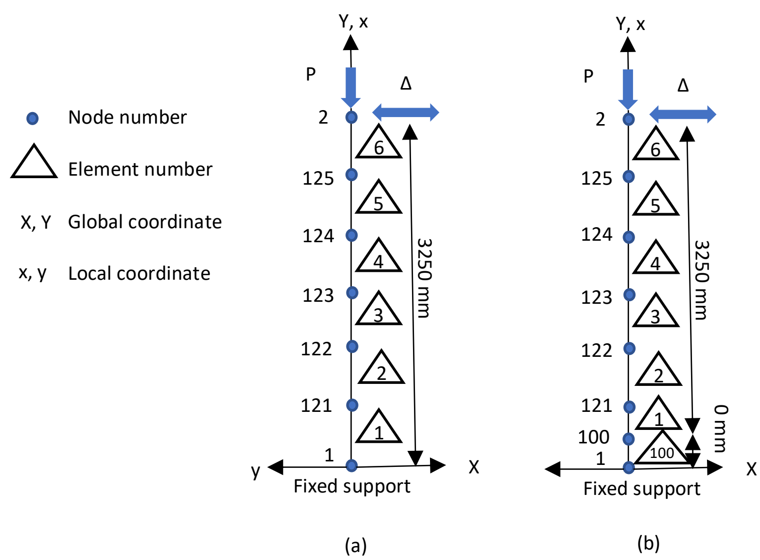

Table 3. Loading Sequences for the Cyclic Loading Test (Chang Et Al. [1])

Cycle Number	1, 2	3, 4	5, 6	7, 8	9, 10	11, 12	13, 14	15, 16	17, 18	19, 20
Drift Ratio (%)	0.25	0.50	0.75	1.00	1.50	2.00	3.00	4.00	5.00	6.00
Displacement (mm)	8.125	16.25	24.38	32.50	48.75	65.00	97.50	130.0	162.5	195.0

Figure 7. Hysteresis Curves from Nonlinear Static Cyclic Pushover Analysis for (a) Model 1 (Excluding Bond-Slip) and (b) Model 2 (Including Bond-Slip)

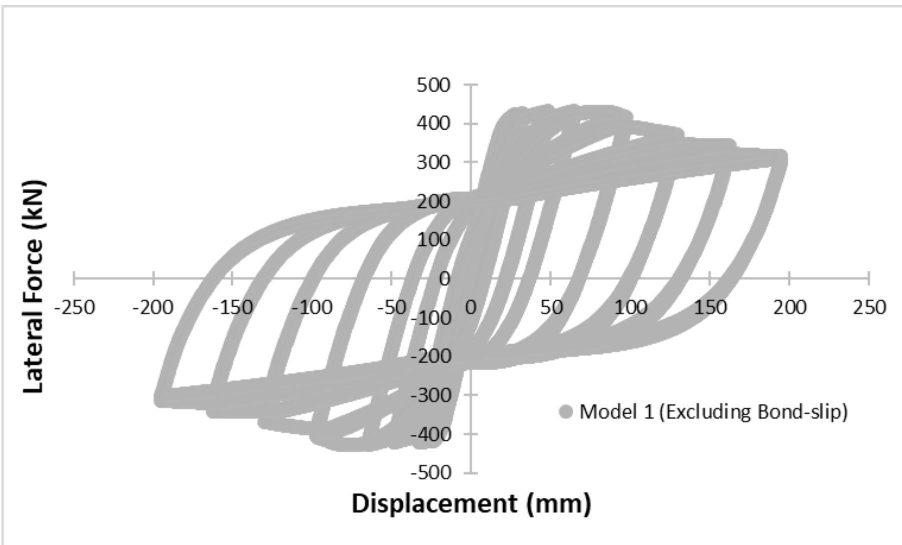

(a)

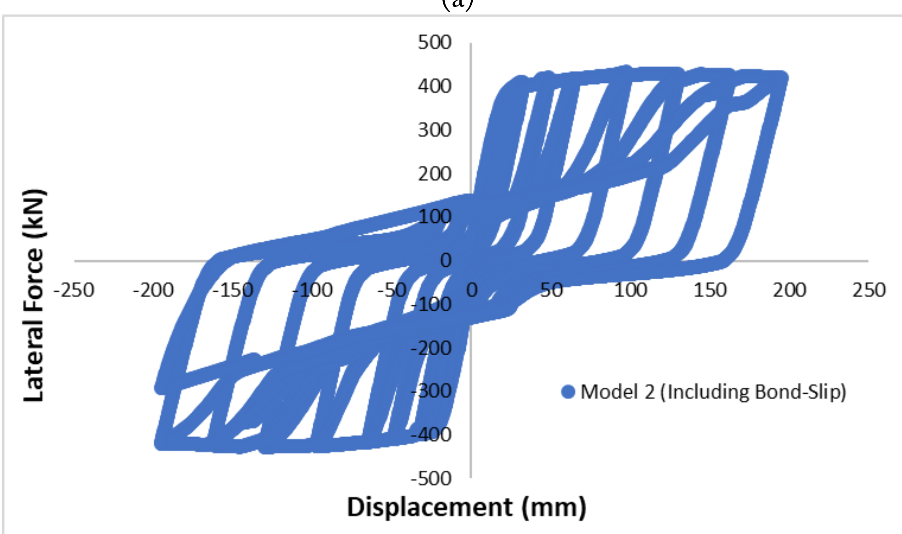

(b)

Table 4. Nonlinear Static Pushover Analysis Results for Model 1 and Model 2 [25]

Model No.	Δy (mm)	Δmax (mm)	$\mu\Delta$,capacity	Fy (kN)
1	19.10	141.0	7.38	384.0
2	22.10	143.0	6.47	384.0

F_y: yield force

6. Nonlinear Response History Analysis

6.1 Description and Scaling of Near-Fault Horizontal Ground Motion

Model 1 and Model 2 were modeled with a single degree of freedom (SDOF) structure with a constant axial compressive load of P = -680 kN. The earthquake selected for the nonlinear response history analysis (RHA) is from station TCU075 during the Chi-Chi earthquake, which demonstrated a pulse-like velocity waveform. This ground motion was used on Specimen B of Chang et al.'s research [1]. The pseudo-dynamic test results of Specimen B by Chang et al. [1] were compared and calibrated with the simulation results by the proposed finite element models 1 and 2 in this research. The earthquake was labeled as: Chi-Chi, Taiwan, record sequence #: 1510, event name: RSN1510_CHICHI_TCU075-E, unscaled PGA: 0.233 g, and unscaled time duration: 90 s.

The recorded time history (s) of ground acceleration (g), ground velocity (cm/s), and ground displacement (cm) are shown in Figure 9. It is noted that the peak ground acceleration was scaled to 0.8 g. In addition, the time was compressed due to the similitude law. This scaled ground acceleration was applied to both models, as shown in Figure 8, with a damping ratio of 5%. Notably, Figure 9 illustrates having a pulse-like velocity waveform and a large pulse near the beginning of the velocity time history.

Figure 8. Nonlinear RHA Due to Horizontal Ground Motion for (a) Model 1 (Excluding Bond-Slip) and (b) Model 2 (Including Bond-Slip)

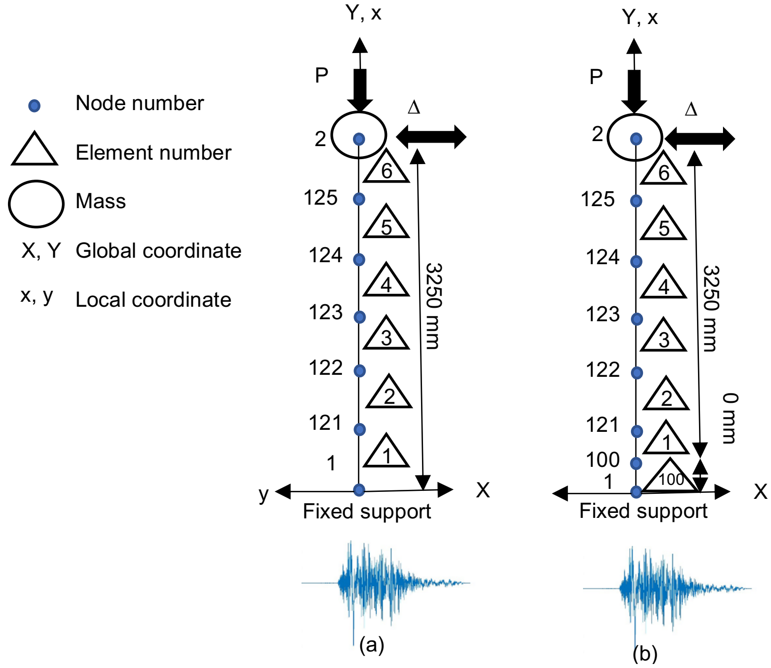

Figure 9. Scaled Horizontal Ground Motion Record from Station TCU075: (Top) Ground Acceleration (G) Over Time (S); (Middle) Ground Velocity (Cm/S) Over Time (S); (Bottom) Ground Displacement (Cm) Over Time (S)

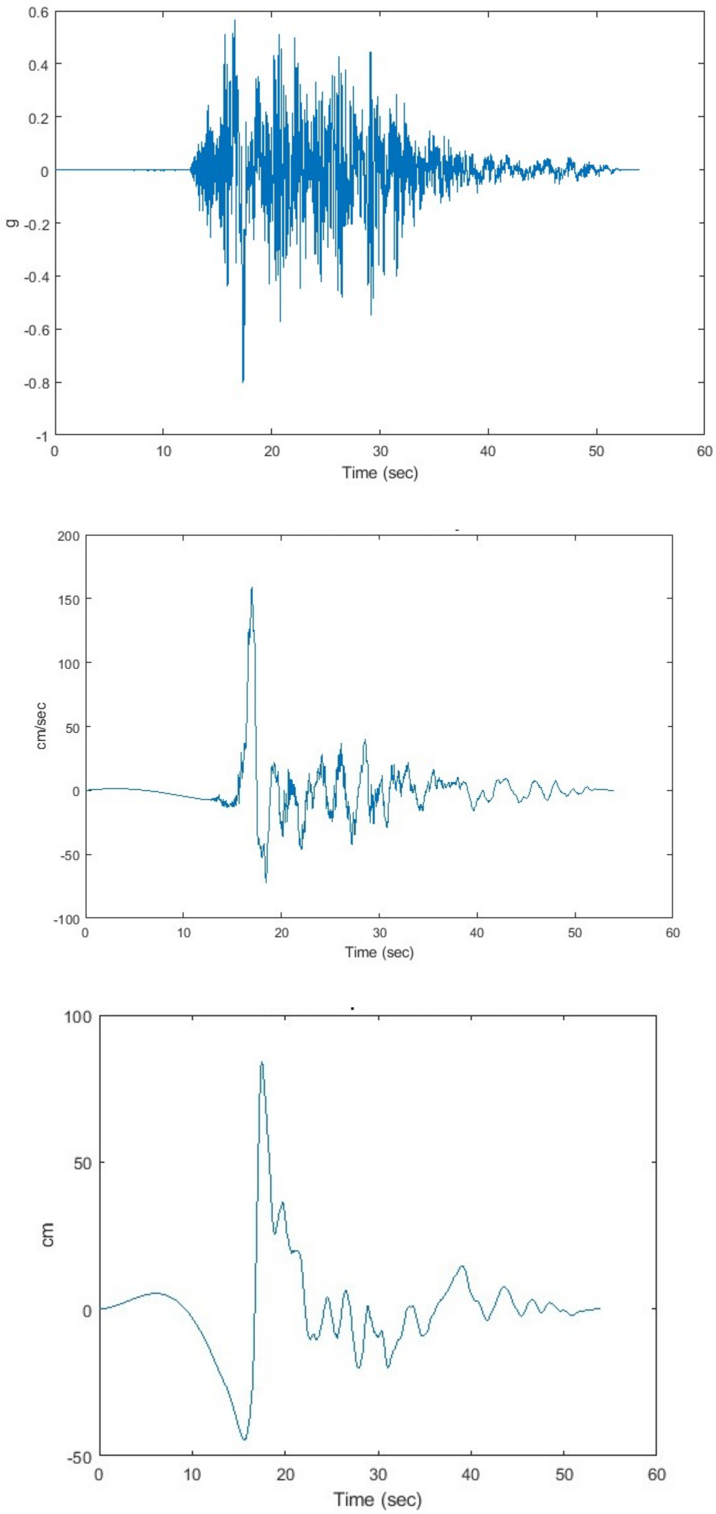

6.2 Moment-Curvature Analysis for the RC Critical Cross Section

The moment-curvature analysis of the RC critical cross section was performed on OpenSees and is shown in Figure 10. The applied constant axial compressive load (P = -680 kN), nominal moment (M_n = 1268 kN-m), yield curvature (ϕ_y = 0.00000621/mm), ultimate moment (M_u = 1486 kN-m), and ultimate curvature (ϕ_u = 0.00006/mm) were directly derived from the bilinear approximation of the moment–curvature curve of the RC critical cross section located at the base of the RC bridge column.

Figure 10. Moment-Curvature Analysis for the RC Critical Cross Section about the Strong Axis (Local Z-Axis) with an Axial Compressive Load of P = -680 Kn

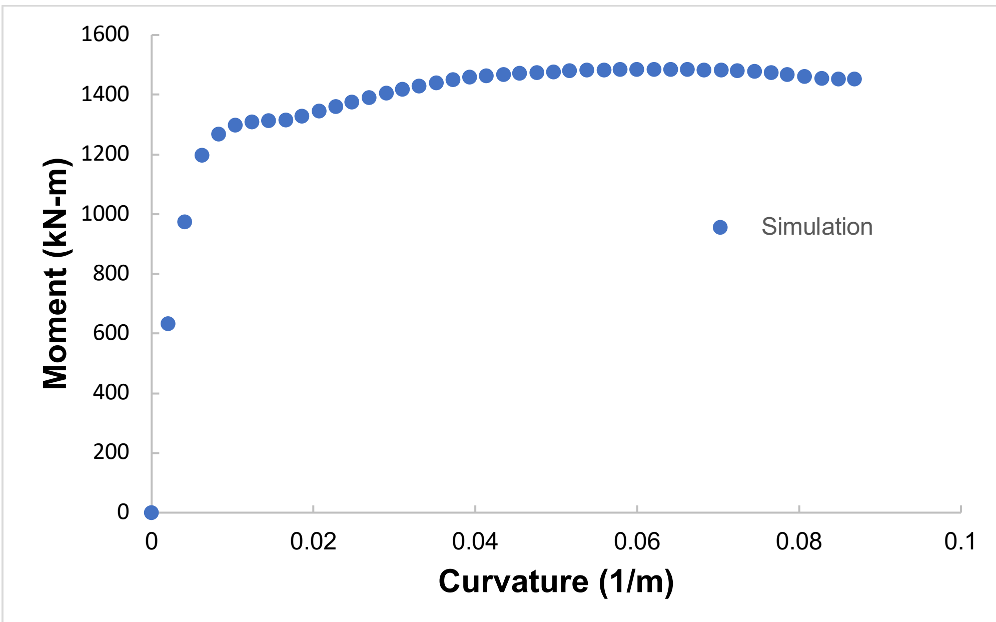

6.3 Ductility Capacity

The plastic rotation capacity and the ductility capacity are interdependent, and were assessed as follows.

Plastic rotation capacity was derived with bilinear approximation of the moment-curvature of the critical cross-section. The curvature ductility capacity was calculated as $\mu_{\phi,capacity} = \phi_u/\phi_u$ = 9.66. The plastic rotation capacity is the difference between the rotation at the ultimate load and at a load causing the yielding of the reinforcement: $\phi_p = \phi_u - \phi_y$ = 0.00005379/mm. The plastic curvature is assumed to be constant over the equivalent plastic hinge length (L_p = 435.56 mm). The plastic rotation is computed as $\theta_p = L_p\ (\phi_u - \phi_y)$ = 0.023 rad.

The member displacement ductility capacity was 4.35 which was defined as follows:

$$\mu^*_{\Delta,\text{capacity}} = \frac{\Delta_u}{\Delta_y} = 1 + \frac{\Delta_p}{\Delta_y} \quad (11)$$

$$= \frac{M_u}{M_n} + 3(\mu^*_{\Delta,\text{capacity}} - 1)\, \frac{L_p}{L}(1 - 0.5\frac{L_p}{L})$$

Where the plastic displacement Δp = 73.51 is computed as:

$$\Delta_p = \left(\frac{M_u}{M_n} - 1\right)\Delta_y + L_p(\phi_u - \phi_y)(L - 0.5L_p) \quad (12)$$

And the yield displacement was determined as followed:

$$\Delta_y = \frac{\phi_y L^2}{3} = 21.9\, mm \quad (13)$$

6.4 Ductility Demands

Three different ductility coefficients were computed to determine the ductility demands [32]: (1) system displacement ductility demand μ_Δ; (2) member displacement ductility demand μ^*_Δ; and (3) curvature ductility demand μ_ϕ.

The system displacement ductility demand μ_Δ is computed as follows:

$$\mu_\Delta = \Delta_{max}/\Delta_y \quad (14)$$

The yield displacement Δ_y was derived from nonlinear cyclic static pushover analyses, and the maximum displacement Δ_{max} was determined from nonlinear RHA.

The member displacement ductility demand μ^*_Δ is computed as follows:

$$\mu^*_\Delta = 1 + \Delta_p/\Delta^*_y = 1 + (\Delta_{max} - \Delta_y)/\Delta^*_y \quad (15)$$

The yield displacement $\Delta^*_y = \phi_y L^2/3$ results from structural deformation above the plastic hinge where L is the length (height) of the bridge column. The yield curvature of the critical cross section ϕ_y was determined from full moment–curvature analysis.

(3) Curvature ductility demand in the plastic hinge region $\mu_{\phi,\text{hinge}}$ is computed as follows:

$$\mu_{\phi,\text{hinge}} = \frac{\phi_u}{\phi_y} = \frac{\phi_p + \phi_y}{\phi_y} = 1 + \frac{\phi_p}{\phi_y} \quad (16)$$

where $\theta_p = (\Delta_{max} - \Delta_y)/L$; $\phi_p = \theta_p/L_p$; L_p is the plastic hinge length.

The arrival of a pulse-like velocity waveform of the near-fault ground motion caused pulse-like maximum structural responses. The responses of the RC bridge column under near-fault ground motion were characterized by one or a few large hysteretic cycles. The maximum base flexural moment demand was 1483 kN-m and 1270 kN-m of Models 1 and 2, respectively, which was less than the ultimate moment capacity M_u = 1486 kN-m. The system displacement ductility capacity $\mu_{\Delta,capacity}$ was 7.38 for Model 1 and 6.47 for Model 2, and the highest system displacement ductility demand μ_Δ was 2.62 for Model 1 and 2.85 for Model 2. Table 5 summarizes the comparisons of the simulation results by nonlinear RHA and pseudo-dynamic testing by Chang et al. [1].

6.5 Discussions of Nonlinear RHA Results

Comparisons between the simulated lateral force vs. lateral displacement hysteresis curves of Model 1 and Model 2 from nonlinear RHA and the hysteretic responses of Specimen B by Chang et al. [1] are shown in Figure 11. Figure 11a shows the simulation results of Model 1 (excluding bond-slip) which overestimated the lateral stiffness and underestimated the lateral deflection of the RC bridge column in comparison to experimental test results. Model 1 demonstrated having an unsymmetrical hysteresis curve, as shown in Figure 11a. On the other hand, Model 2 developed symmetrical hysteresis curves, as shown in Figure 11b. Model 2 (including bond-slip) had a less saturated hysteretic loop and a stronger pinching effect due to bond-slip in comparison to Model 1 (which excluded bond-slip). Additionally, Figure 11 also shows that the maximum seismic responses of RC bridge columns under near-fault motion were characterized by one or a few large hysteretic cycles. Overall, the hysteresis curve of Model 1 aligns better with experimental data.

The ductility capacities and ductility demand collected from nonlinear RHA are outlined in Table 5. The curvature, system displacement, and member displacement ductility demand-capacity ratio in the plastic hinge region are all less than 1.0 for Specimen B, indicating that the applicable ductility capacities of this RC bridge column were not fulfilled. As such, the simulation results demonstrated that this RC bridge column (Specimen B) could withstand the chosen near-fault ground motion, which aligned positively with pseudo-dynamic test results by Chang et al. [1].

Figure 11. Comparison of Hysteresis Curves Between Nonlinear RHA Results and Pseudo-Dynamic Tests by Chang Et Al. [1] for (a) Model 1 (Excluding Bond-Slip) and (b) Model 2 (Including Bond-Slip)

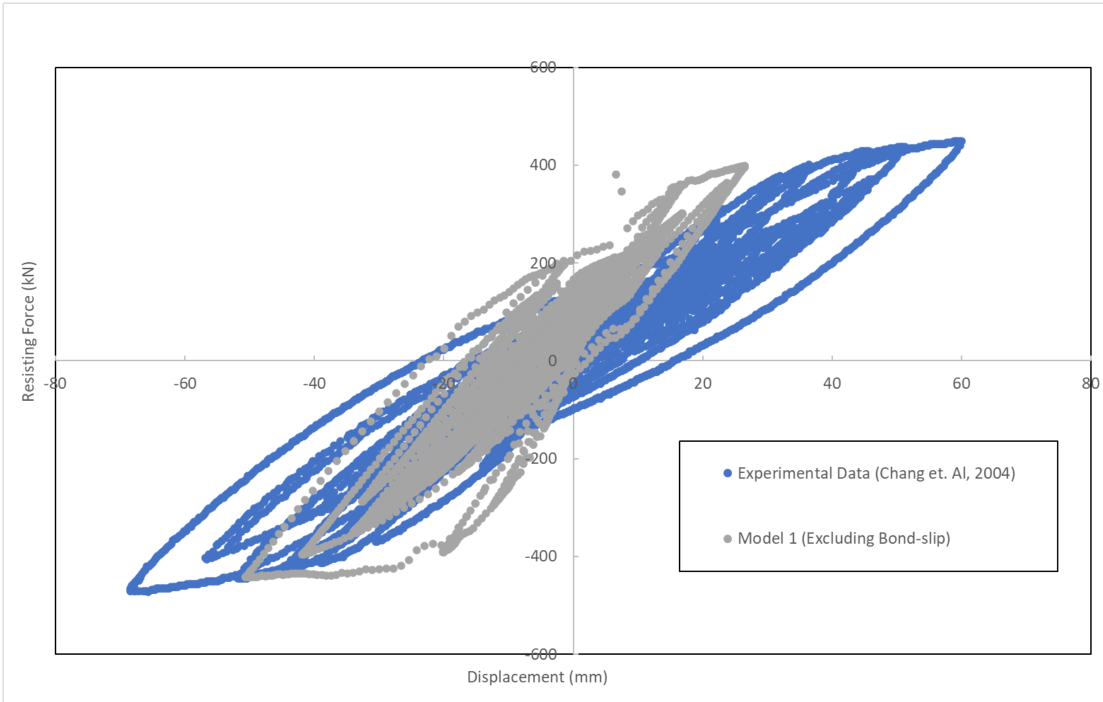

(a)

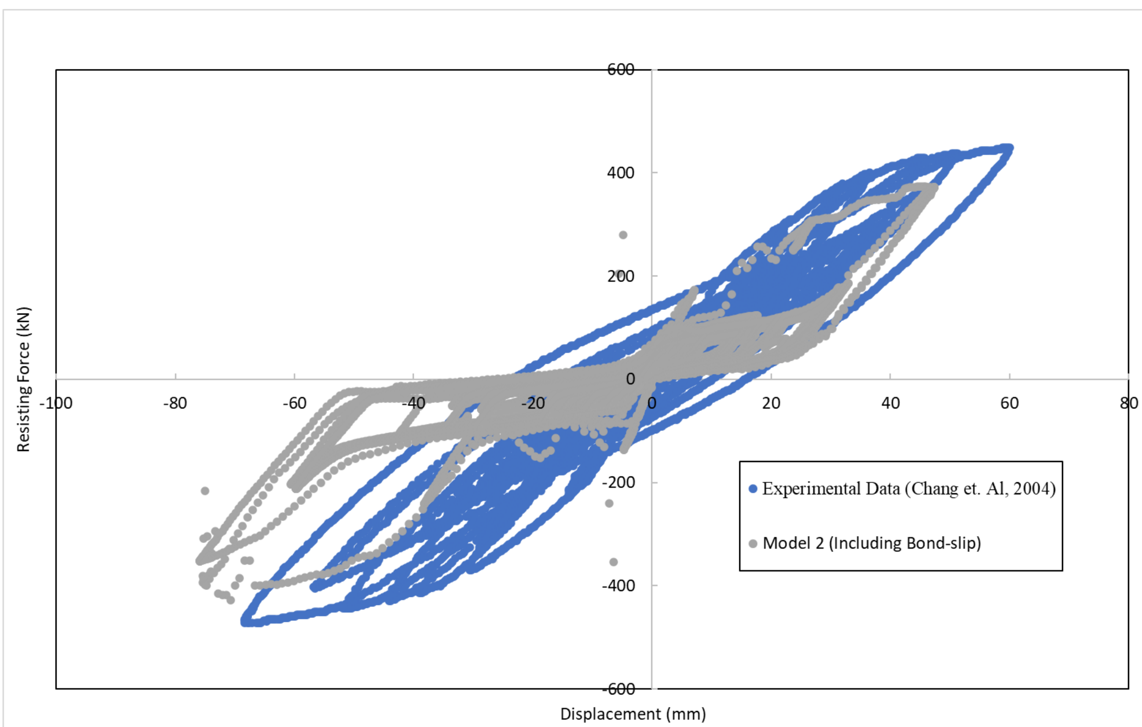

(b)

Table 5. Comparisons of Nonlinear RHA Results and Pseudo-Dynamic Testing by Chang et al. [1]

Model No.	T_n (s)	Max. acceleration (g)	Δ_{max} (mm)	$\frac{(\Delta_{max,top})_{simulation}}{(\Delta_{max,top})_{experimental\ t}}$ (%)	$M_{max,base}$ (kN-m)	$\frac{(M_{max,base})_{simulation}}{(M_{max,base})_{experimental\ te}}$
1	0.344	0.154	49.95	73.10	1483.00	94.88
2	0.351	0.141	63.01	92.21	1270.00	81.25
Pseudo-dynamic test	N/A	N/A	68.33	100.00	1563.00	100.00
Model No.		$\Delta_{residual}$ (mm)	μ_Δ	$\frac{(\mu_\Delta)_{simulation}}{(\mu_\Delta)_{experimental\ test}}$(%)	μ^*_Δ	$\mu_{\phi,hinge}$
1		7.36	2.62	147.19	2.41	4.51
2		0.06	2.85	160.11	2.87	5.65
Pseudo-dynamic test		N/A	1.78	100.00	N/A	N/A

T_n: vibration period
$M_{max,base}$: maximum base moment
$\Delta_{residual}$: residual displacement at bridge column top

7. Damage Indices

The RC bridge pier's damage values at each step of the loading history are calculated according to the proposed damage index assessment, and the results are shown in Figures 12–14. The graphs shown below compare the concrete damage (Figure 12), steel strain damage (Figure 13), and section damage index (Figure 14) of Models 1 and 2. The concrete damage (D_c) of Model 1 reached 0.1 after 16.575 seconds, while Model 2 remained at a consistent 0.0 throughout the whole run time. The strain damage (D_{SS}) graph shows Model 1 has greater damage values than Model 2 with D_{ss} = 0.1930 for Model 1 and D_{ss} = 0.1145 for Model 2 as their maximum strain values. The maximum section damage index was D_{sec} = 0.1930 for Model 1 and D_{sec} = 0.1145 for Model 2. The proposed models achieved the onset of spalling with an onset of cracks and a yielding of longitudinal reinforcement but remained operational as per Table 2 [24]. The damage description of the proposed models aligns closely with the experimental results of Specimen B by Chang et al. [1], where the yielding of some longitudinal bars was detected, but there was no buckling among them. However, flexural cracks were found, and slight spalling of concrete cover was also observed. Overall, the damage indices show that when bond-slip is considered, damage is underestimated as the bar strain simulated by Model 2 (including bond-slip) was smaller than Model 1 (excluding bond-slip). Therefore, Model 1 is most optimal.

Figure 12. Concrete Samage (D_c) of Model 1 and Model 2

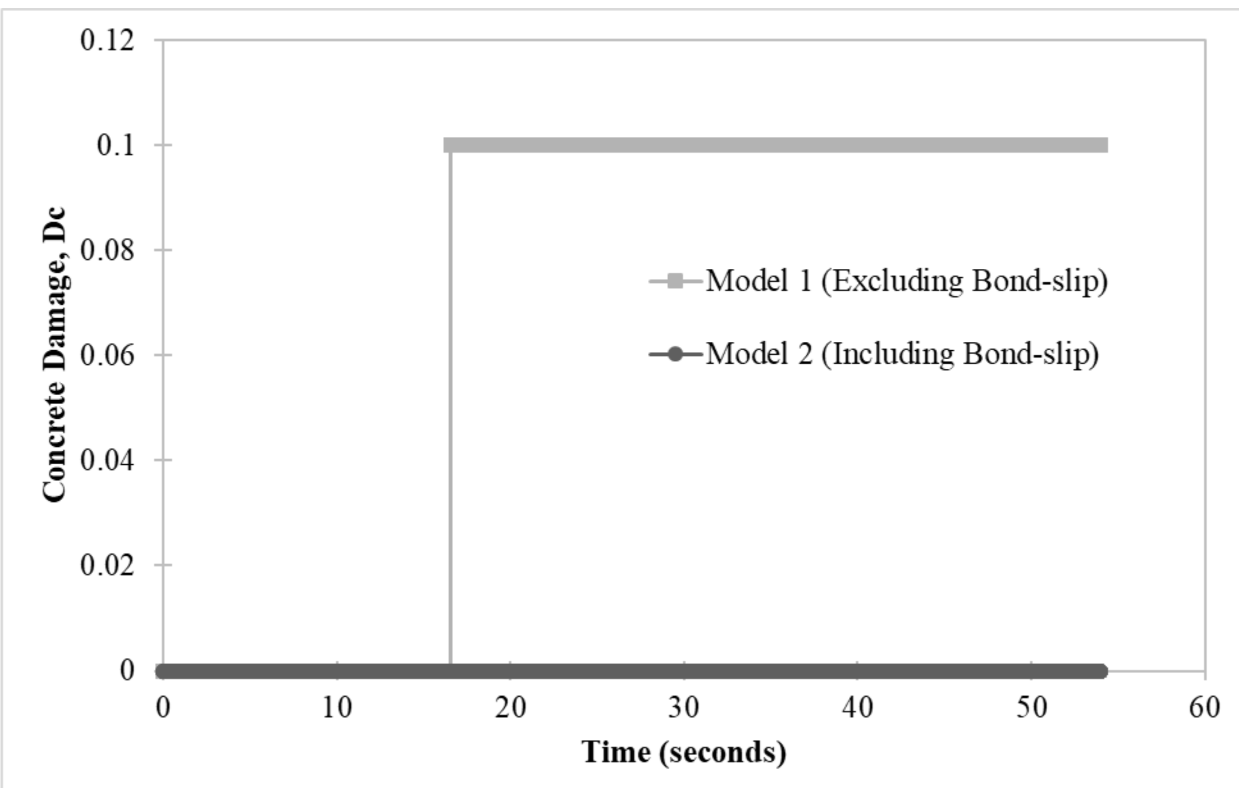

Figure 13. Steel Strain Damage (D_{SS}) of Model 1 and Model 2

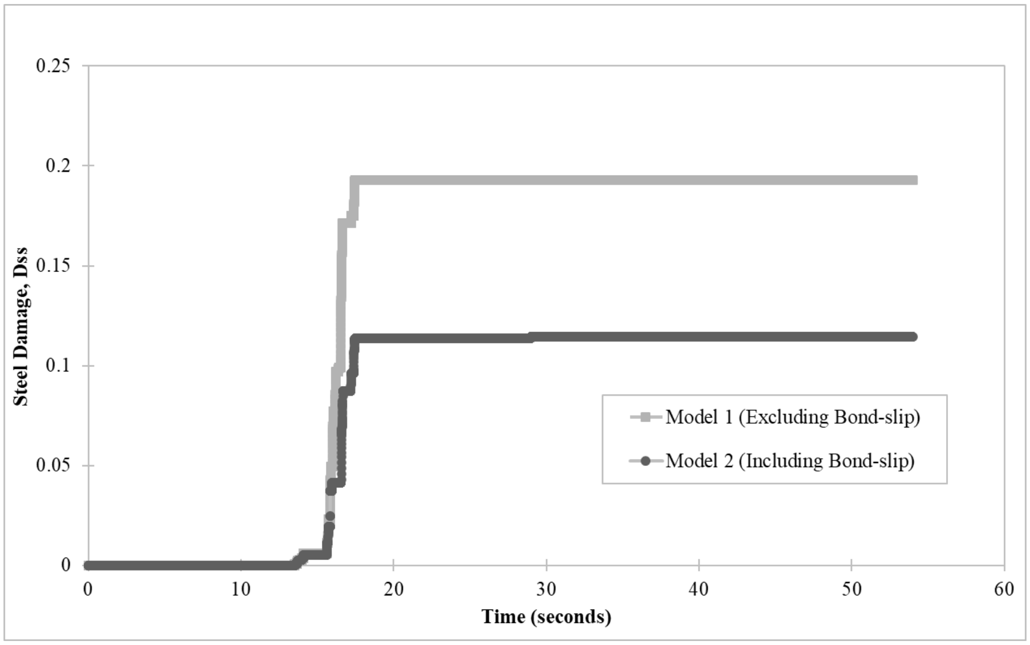

Figure 14. Section Damage Index (D_{sec}) of Model 1 and Model 2

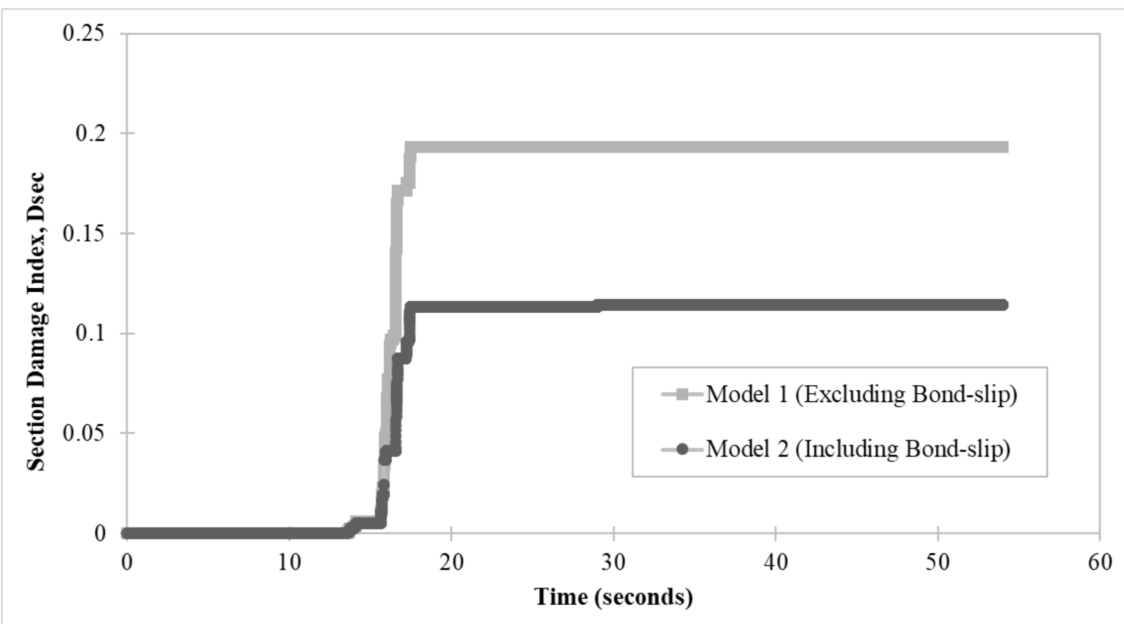

8. Summary & Conclusions

This research investigated the seismic performance of RC single-column pier-supported bridges under near-fault ground motion through the use of ductility coefficients and damage indices. Two different FEMs were proposed: Model 1 (excluding bond-slip) and Model 2 (including bond-slip) to study and compare their ductile responses and damage indices. The proposed models assessed seismic damage of RC bridge columns based on ductility demand versus capacity, as well as through the use of damage indices. The damage indices show that when bond-slip is concerned, damage is underestimated. Therefore, Model 1 (excluding bond-slip) is most optimal to assess the seismic performance of RC single-column pier-supported bridges with flexural failure under near-fault ground motion. The proposed damage index can reasonably reflect the damage states at the onset of spalling, significant spalling, bar buckling, and failure in accordance with the experimental results.

Bond-slip noticeably affects the seismic response of RC single-column pier-supported bridges when comparing the numerical simulation results by proposed fiber-based finite element models and experimental observations. The simulation results of Model 1 (excluding bond-slip) are closely aligned with the pseudo-dynamic test results under near-fault ground motion on hysteretic responses and damage mechanisms including cover concrete spalling and yielding of longitudinal reinforcing steel bars, the only exception being their underestimating of the lateral deflection of the RC bridge column. Model 2 (including bond-slip) underestimated the ultimate lateral load resistance, longitudinal reinforcing steel bar strain, and cover concrete strain as well as slightly underestimating the lateral deflection of the RC bridge column when compared with the pseudo-dynamic results under near-fault ground motion. Further study is needed to support these findings including assessing more experimental data and comparing them with far-fault ground motion. Additionally, the simulation results of the proposed fiber-based damage FEMs showed that pulse-like maximum structural responses—including displacement at the bridge column top, base shear, and base flexural moment—develop with the arrival of pulse-like velocity waveforms of near-fault ground motion. Additionally, the maximum seismic responses of RC bridge piers under near-fault ground motion were represented by one or a few large hysteretic cycles. The pulse-like peak responses of RC bridge piers were primarily due to the pulse-like velocity waveform of the near-fault ground motion.

RC bridge piers designed without adequate ductility capacity undergo premature cover concrete spalling and shear failure due to the unique damage characteristics of near-fault ground motion. Thus, the structural responses and attributes of near-fault ground motion should be considered when designing RC bridge structures located in near-fault regions. The proposed fiber-based damage FEMs are an effective and efficient method to administer preliminary assessments on seismic performance of RC single-column pier-supported bridges. The proposed fiber-based damage FEMs will also help engineers and researchers improve the analysis of RC bridge performance under seismic cyclic loadings and identify what components should be considered when designing bridges in near-fault regions, ultimately supporting the advancement of the structural engineering profession.

Bibliography

1. Chang, Y. S., Li, Y. F., and Loh, C. H. (2004). Experimental study of seismic behaviors of as-built and carbon fiber reinforced plastics repaired reinforced concrete bridge columns. *J Bridge Eng ASCE* 9(4): 391–402.

2. Loh, C. H., Wan, S., and Liao, W. I. (2002). Effects of hysteretic model on seismic demands: consideration of near-fault ground motions. *Struct Des Tall Build* 11: 155–169.

3. Ansari, M., Daneshjoo, F., and Mohammadi, M. S. (2017). On estimation of seismic residual displacements in reinforced concrete single column bridges through force-displacement method. *Int J Civil Eng* 15: 473–486.

4. Yi, W. J., Zhou, Y., Hwang, H. J., Cheng, Z. J., and Hu, X. (2018). Cyclic loading test for circular reinforced concrete columns subjected to near-fault ground motion. *Soil Dyn Earthq Eng* 112: 8–17.

5. Cao, V.V. (2019). Characterization of near-fault effects on potential cumulative damage of reinforced concrete bridge piers. *Int J Civil Eng* 17: 1603–1618.

6. Xia, C., and Liu, C. (2020). Influence of the multi-pulse near-fault earthquake motion on the seismic risk evaluation for reinforced concrete bridge. *Nat Hazards* 102: 759–782.

7. Pang, Y. T., Cai, L., and Zhong, J. (2020). Seismic performance evaluation of fiber-reinforced concrete bridges under near-fault and far-field ground motions. *Structures* 28: 1366–1383.

8. Seyed Ardakani, S. M., Saiid Saiidi, M., and Somerville, P. (2021). Residual drift spectra for RC bridge columns subjected to near fault earthquakes. *Earthq Eng Eng Vib* 20: 193–211.

9. Mergos, P. E., and Kappos, A. J. (2013). A combined local damage index for seismic assessment of existing RC structures. *Earthquake Engineering and Structural Dynamics* 42(6): 833–852.

10. Park, Y., and Ang, A. H. (1985). Mechanistic seismic damage model for reinforced concrete. *J Struct Eng* 111(4): 722–39.

11. Park, Y., Ang, A. H., and Wen, Y. (1987). Damage-limiting aseismic design of buildings. *Earthq Spectra* 3(1): 1–26.

12. Heo, Y., and Kunnath, S. K. (2013). Damage-based seismic performance evaluation of reinforced concrete frames. *Int J Concr Struct Mater* 7(3): 175–82.

13. Kratzig, W., and Meskouris, M. (1987). Nonlinear seismic analysis of reinforced concrete frames. In: Vogel, Brandes (Eds.), *Earthquake Prognostics*, Verlag Friedr, Vieweg and Sohn, Braunschweig: 453–62.

14. Williams, M. S., and Sexsmith, R. G. (1995). Seismic damage indices for concrete structures: a state-of- the-art review. *Earthq Spectra* 11(2): 319–49.

15. Babazadeh, A., Burgueño, R., and Silva, P. F. (2015). Use of 3d finite-element models for predicting intermediate damage limit states in rc bridge columns. *J Struct Eng* 141(10): 04015012:1-11.

16. Kashani, M. M., Lowes, L.N., Crewe, A. J., and Alexander, N. A. (2016). Nonlinear fiber element modelling of rc bridge piers considering inelastic buckling of reinforcement. *Eng Struct* 116: 163–77.

17. Su, J., Dhakal, R. P., and Wang, J. (2017). Fiber-based damage analysis of reinforced concrete bridge piers. *Soil Dynamics and Earthquake Engineering* 96: 13–34. https://doi.org/10.1016/j.soildyn.2017.01.029.

18. Stone, W. C., and Taylor, A. W. (1993). *Seismic performance of circular bridge columns designed in accordance with aashto/caltrans standards*. NISIT building Science Series 170, National Institute of Standards and Technology, Gaithersburg, MD.

19. Stone, W. C., and Taylor, A. W. *Performance evaluation database for concrete bridge components and systems under simulated seismic loads*. PEER Report 1999/11, Pacific Earthquake Engineering Research Center, Berkeley, CA; 1999.

20. Goodnight, J. C., Kowalsky, M. J., and Nau, J. M. (2016). Strain limit states for circular RC bridge columns. *Earthquake Spectra* 32(3): 1627–1652.

21. McKenna, F., Fenves, G. L., and Scott, M. H. (2000). *Open system for earthquake engineering simulation*. University of California, Berkeley, CA.

22. Sharifi, A., Banan, M., and Banan, M. (2012). A strain-consistent approach for determination of bounds of ductility damage index for different performance levels for seismic design of rc frame members. *Eng Struct* 37: 143–51.

23. Yue, J., Qian, J., and Beskos, D. E. (2016). A generalized multi-level seismic damage model for rc framed structures. *Soil Dyn Earthq Eng* 80: 25–39.

24. Transportation Research Board (TRB). (2013). Performance-based seismic bridge design, Rep. No. Synthesis 440. National Cooperative Highway Research Program, Washington, DC.

25. Ko, Y. F. (2022). Finite Element Analysis of Reinforced Concrete Single-Column Bridge Bent with Flexural Failure Under Near-Fault Ground Motion. *International Journal of Civil Engineering* 20(3): 237–256.

26. Park, R., and Paulay, T. (1975). *Reinforced concrete structures*. Wiley, New York.

27. Girard, C., and Bastien, J. (2002). Finite-element bond-slip model for concrete columns under cyclic loads. *J Struct Eng ASCE* 128(12): 1502–1510.

28. Zhao, J., and Sritharan, S. (2007). Modeling of strain penetration effects in fiber-based analysis of reinforced concrete structures. *ACI Struct J* 104(2): 133–141.

29. Gomes, A., and Appleton, J. (1997). Nonlinear cyclic stress-strain relationship of reinforcing bars including buckling. *Eng Struct* 19(10): 822–826.

30. Dhakal, R. P., and Maekawa, K. (2002). Modeling for postyield buckling of reinforcement. *J Struct Eng ASCE* 128(9): 1139–1147.

31. Paulay, T., and Priestley, M. J. N. (1992). *Seismic design of reinforced concrete and masonry buildings*. Wiley, New York.

32. Priestley, M. J. N., Seible, F., and Calvi, G.M. (1996*). Seismic design and retrofit of bridges*. Wiley-Interscience, New York.

33. Chang, G., and Mander, J. (1994). *Seismic energy-based fatigue damage analysis of bridge columns: part I—evaluation of seismic capacity*. NCEER Technical Report 94-0006.

34. Kunnath, S. K., Heo, Y., and Mohle, J. F. (2009). Nonlinear uniaxial material model for reinforcing steel bars. *J Struct Eng* 135(4): 335–43.

35. Yassin, M. H. M. (1994). *Nonlinear Analysis of Prestressed Concrete Structures under Monotonic and Cycling Loads*. PhD dissertation, University of California, Berkeley, 1994.

About the Authors

Yu-Fu Ko, PhD, PE (Principal Investigator)

Dr. Ko joined the California State University, Long Beach (CSULB) Civil Engineering and Construction Engineering Management Department in Fall 2009. He received his B.S. degree in Structural Engineering from National Taiwan University of Science and Technology and his M.S. and Ph.D. degrees (as an outstanding Ph.D. award recipient) in Civil Engineering, focusing on Structural Mechanics and Structural Engineering/Dynamics from the University of California, Los Angeles (UCLA). Prior to joining CSULB, Dr. Ko was a postdoctoral researcher and lecturer at UCLA and a senior structural design engineer at Englekirk and Sabol Consulting Structural Engineers, Inc. He is a registered Professional Civil Engineer in the state of California. Dr. Ko's areas of research include micro/nano-mechanics modeling of heterogeneous composite materials, micromechanical damage mechanics modeling and associated applications, damage assessment and experimental mechanics of structural materials, nonlinear/linear structural dynamic analysis of structures subjected to earthquake motions, finite element method code-based and performance-based structural design of structures, and seismic retrofitting of existing structures. He has presented at national and international conferences and published research papers in national and international peer-reviewed journals. He actively participates in ASCE, ASME, AISC, ACI, SEAOSC, IACM, USACM, and other national and international societies. He is also a peer reviewer for numerous technical journals.

Jessica Gonzalez, EIT (Research Graduate Assistant)

Jessica Gonzalez is a research graduate assistant working with Dr. Yu-Fu Ko at California State University, Long Beach (CSULB). She received her B.S. in civil engineering from CSULB with Cum Laude degree honors and is currently enrolled as a graduate student working towards her master's degree. She is certified as an Engineer-in-Training (EIT) and is currently employed as a structural designer at RailPros, Inc. Her research interests are finite element modeling of bridges and the seismic analysis of bridge components. Additionally, her software skills include AutoCAD and OpenSees.

MTI FOUNDER

Hon. Norman Y. Mineta

MTI BOARD OF TRUSTEES

Directors

MINETA TRANSPORTATION INSTITUTE